Diffuse-transmission spectroscopy: A structural probe of opaque colloidal mixtures

P.D. Kaplan,* A.D. Dinsmore, and A.G. Yodh

Physics Department, University of Pennsylvania, Philadelphia, Pennsylvania 19104

D.J. Pine

Exxon Research and Engineering Company, Annandale, New Jersey 08801

The wavelength-dependent diffuse transmission through a monodisperse colloidal suspension is shown to provide wave-vector-dependent information about the colloid structure factor. Experiments demonstrate that the spectral fingerprint can be used to distinguish quantitatively samples of different particle sizes, different concentrations, and different interparticle interactions.

PACS number(s): 82.70.Dd, 41.20.Jb, 61.20.−p

I. INTRODUCTION

The average arrangement of particles in a colloidal suspension is one of the most fundamental properties of suspensions and is the key to understanding virtually all physical properties of colloids. Particle diffusion, sedimentation, rheology, and colloidal stability all depend on how the colloidal particles arrange themselves, that is, on colloidal structure. The structure of colloidal suspensions is typically characterized by the pair correlation function, or by its Fourier transform, the static structure factor. The structure factor is particularly useful since it can be measured directly in certain special circumstances by a variety of experimental techniques. For example, colloidal structure can be measured using light scattering if the sample under study scatters light so weakly that light passing through the sample scatters no more than once. Such weak scattering typically occurs, however, only in very dilute samples; scattering can also be made sufficiently weak in exceptional cases where the refractive index of the particles is very closely matched to that of the solvent. Other traditional probes of colloidal structure not subject to these limitations include small angle x-ray scattering using a synchrotron (appropriate for colloids consisting of particles smaller than 0.1 μm) and small angle neutron scattering using a nuclear reactor to study systems in which isotopic substitution is practical. Many useful and interesting colloids, however, are neither dilute, nor index matched, nor small in size, nor easily amenable to isotopic substitution. Such colloids typically exhibit a very high degree of multiple light scattering and appear white, like milk or white paint. These optically opaque colloids make up the vast majority of practical suspensions. Until very recently, no convenient probe of the structure of these systems was readily available.

In this paper, we introduce a light scattering technique which, hereafter, we will refer to as diffuse-transmission spectroscopy (DTS). Diffuse-transmission spectrospy *employs* multiple scattering to probe the structure of optically opaque colloidal suspensions with weak photon absorption. Diffuse-transmission spectrospy uses an incandescent lamp and monochrometer to obtain a transmission spectrum from which structural information about the sample can be deduced. To demonstrate this technique, we present measurements from concentrated suspensions of polystyrene spheres in water. We demonstrate that diffuse transmission data provide a spectral fingerprint that is useful for particle sizing, determining the volume fraction, and monitoring of interparticle potentials. The DTS data set is not adjustable and allows direct comparison with structural models.

The cornerstone of our approach is the diffusion approximation for photon transport in highly multiple-scattering media. In the diffusion approximation, photon transport is characterized by a single parameter, the photon transport mean free path l^*. We will review the connection between interparticle structure and l^*, and demonstrate that the connection can be exploited to probe colloidal structure in a transmission measurement. We begin, however, with a brief overview of the aspects of traditional single-scattering experiments that are relevant to our subsequent discussions of the multiple scattering problem.

II. STRUCTURAL MEASUREMENTS USING SINGLE SCATTERING

In single-scattering experiments, the length scale at which colloidal structure is probed is set by the inverse of the scattering wave vector q^{-1}. The scattering wave vector $\mathbf{q}$ is the difference between the incident and scattered wave vectors $\mathbf{k_0}$ and $\mathbf{k}_f$ from a single-elastic-scattering event. It is easy to vary q by changing the scattering angle θ:

$$q \equiv |\mathbf{q}| = |\mathbf{k}_f - \mathbf{k_0}| = 2k_0 \sin(\theta/2) , \qquad (1)$$

where $k = 2\pi/\lambda$ for photons with wavelength λ in the

---

*Present address: NEC Institute, 4 Independence Way, Princeton, NJ 08540.

scattering medium. By varying the scattering angle θ from $0°$ to $180°$, one can, in principle, access wave vectors between $q = 0$ and $q = 2k_0$.

In monodisperse colloids, the intensity of light scattered through a wave vector q can be written as a product of the form factor $F(q, k_0 a)$, which describes scattering from an isolated particle of diameter a, and the structure factor $S(q)$, which describes the correlations in positions between particle centers [see Fig. 1(a) and Eq. (1)], i.e.,

$$I(q) = F(q, k_0 a) S(q) . \qquad (2)$$
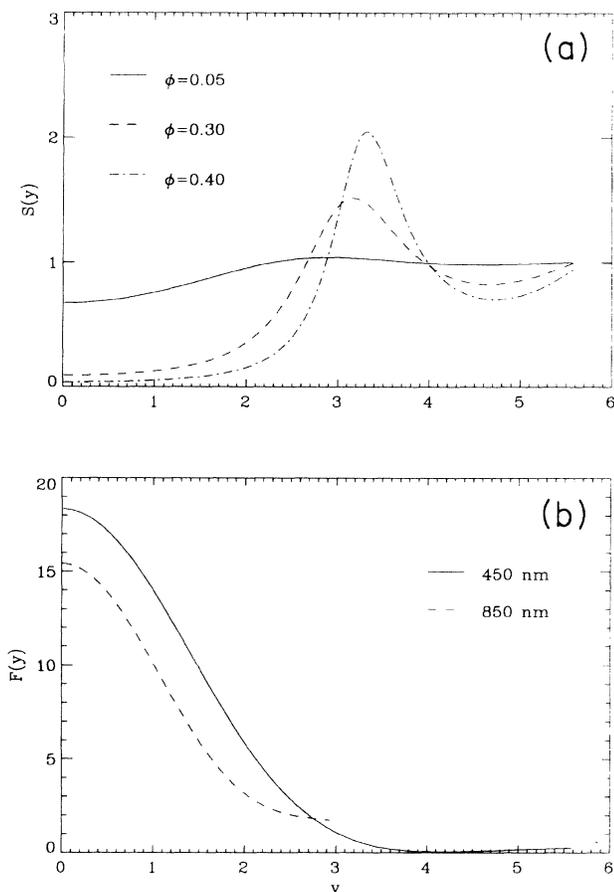
FIG. 1. (a) Plot of the structure factor (calculated from Percus-Yevick theory for a hard-sphere potential) at various volume fractions ϕ vs dimensionless wave vector $y = qa$. (b) Plot of the form factor (calculated from Mie theory) vs y at wavelengths of 450 nm and 850 nm for a 205-nm diameter particle. The form factor at 850 nm has been magnified by a factor of 50 for visual comparison with the form factor at 450 nm. Note that the form factor for scattering through angles between $0°$ and $180°$ covers a different range of scattering wave vectors at each wavelength because the largest dimensionless scattering wave vector is $4\pi a/\lambda$. Scattering from collections of particles depends on the product $F(y)S(y)$ of the curves in (a) and (b); thus, scattering at different wavelengths will depend on different parts of the structure factor. In this paper, we explore ways to use this fact to extract information about the structure factor from scattering data from opaque, multiple-scattering samples.

The form factor of micron-sized particles depends on the contrast in index of refraction between particle and solvent, the ratio of the particle radius to the photon wavelength $k_0 a$, the photon polarization, and the scattering wave vector q. The dependence of F on $k_0 a$ is usually not written explicitly; however, this dependence is critical for understanding the technique described in this paper. For scattering problems with $k_0 a$ of order unity, the form factor must be computed using Mie theory [1]. The structure factor is related to real space particle positions r_i, according to

$$S(\mathbf{q}) = (1/N)\left\langle \sum_{i,j} e^{i\mathbf{q}\cdot(\mathbf{r}_i - \mathbf{r}_j)} \right\rangle - N\delta(\mathbf{q}) , \qquad (3)$$

where N is the number of particles. In Fig. 1(b), we plot the Mie scattering form factor as a function of dimensionless wave vector $y \equiv qa$ at two different optical wavelengths (i.e., different values of $k_0 a$). The value of y ranges from zero to $2k_0 a$, corresponding to the full range of wave vectors that could be accessed in a single-scattering experiment.

Measurements of the scattered intensity as a function of scattering angle (and hence q) provide explicit information about colloid structure. In fact, light scattering is useful in a wide variety of complex fluids which exhibit structures on length scales comparable to the wavelength of light, so long as multiple scattering can be neglected. In the next section, we address the possibility of probing the structure of colloidal suspensions (and, therefore, other complex fluids) using light scattering in samples which exhibit a very high degree of multiple scattering.

III. DIFFUSE-TRANSMISSION SPECTROSCOPY: STRUCTURAL MEASUREMENTS USING MULTIPLE LIGHT SCATTERING

In multiple-scattering experiments, photons scatter many times through many different scattering angles (and wave vectors) before being detected. Therefore, we expect structural information imprinted on the multiply-scattered light to be smeared out relative to the single-scattering case. Moreover, variation of the angle between incident and exiting light beams provides little additional structural information when photons have traveled a distance greater than $5l^*$ through the sample. Nevertheless, it is still possible to obtain significant structural information about the suspension from multiple scattering. Our strategy to obtain the desired length-scale or wave-vector resolution is to change the *wavelength* of the incident light and detect *all* the light transmitted through the sample (i.e., all scattering angles). We describe our approach below.

In order to obtain useful structural information about a colloidal suspension from multiply-scattered light, we require a model for light propagation in the highly multiple-scattering limit. While there are many approaches available to describe photon transport in random media, the simplest and most generally useful is the photon diffusion

approximation. This approach has been used recently to describe photon transport in a wide variety of systems with a great deal of success. Some examples include photon transport in clouds [2], model biological tissue [3,4], foams [5], paper [6], dairy products [7], and colloids [8–11].

In the diffusion approximation, one assumes that each photon scatters many times and that its transport through the medium can be described as a random walk. The average distance between scattering events (the scattering mean free path) is $l = 1/\rho\sigma_{sc}$, where ρ is the number density of scattering particles, and σ_{sc} is the scattering cross section per particle. For the general case of scattering from correlated groups of identical particles,

$$\sigma_{sc} = \frac{1}{k_0^2} \int_0^{2k_0 a} F(y, k_0 a)\, S(y)\, y\, dy\,, \qquad (4)$$

where y is the dimensionless scattering wave vector qa. This form for the scattering cross section is obtained by integrating the product of the structure and form factors over all accessible scattering angles. The form factor is generally peaked at small angles (small q). As a consequence, the direction of propagation of a photon is not randomized by a single-scattering event, but is randomized after many-scattering events. There is a longer length scale, however, over which the direction of propagation of a photon is randomized. This length scale is called the transport mean free path l^*. It corresponds to the length of one step in the random walk executed by the photon. The diffusion approximation is valid so long as there are many random walk steps in any light path under consideration. Conservatively, this is true for samples thicker than than $10l^*$ [12]. The transport mean free path l^* is related to the average distance between scattering events l through average value of the cosine of the scattering angle, $\langle\cos(\theta)\rangle$ [1,9,13]

$$\frac{l^*}{l} = \frac{1}{1 - \langle\cos(\theta)\rangle}\,. \qquad (5)$$

For isotropic scattering, $\langle\cos(\theta)\rangle = 0$ and $l^* = l$. For scattering increasingly peaked in the forward direction, $\langle\cos(\theta)\rangle$ becomes closer to 1 and l^* becomes increasingly greater than l. This result (5) is valid as long as structural correlations in the sample are short compared to l. For example, we do not expect (5) to apply to transport through a colloidal crystal. Combining Eqs. (4) and (5), we arrive at an expression for the transport mean free path length in a monodisperse suspension,

$$\frac{1}{l^*} = \frac{\pi\rho}{(k_0 a)^4 k_0^2} \int_0^{2k_0 a} y^2\, F(y, k_0 a)\, S(y)\, y\, dy\,. \qquad (6)$$

Thus, the photon transport mean free path l^* is calculated by integrating over the *product* of the form factor and the structure factor weighted by y^3. The form factor is well known for spherical particles. Here, we wish to study the structure factor. In the diffusion approximation, we envision the photons as scattering from a sequence of correlated particle clusters [14]. It should be noted that (6) is valid only when structural corre-

lations extend over lengths that are small compared to l^*. In the present case, $l^* \gtrsim 7$ μm or at least 14 ball diameters, so this condition is always satisfied. A more restrictive condition is that the mean distance between scattering events l exceeds the distance over which there are structural correlations. This is always true for the 205- and 299-nm particles where $l \gtrsim 3$ ball diameters. However, in the case of the 460-nm particles, l^* is only greater than 3 for λ longer than 700 nm, and we cannot be sure that (6) is true at shorter wavelengths. We note, however, that diffusing-wave spectroscopy (DTS) measurements have been performed in highly concentrated systems for which the more restrictive condition is violated [10,11,15,16]. In these cases experiment and theory agree to within the experimental error of 10% suggesting that the more restrictive condition is perhaps too restrictive.

To gain some physical insight into the connection between structure and multiple light scattering, we plot the structure factor for hard spheres in Fig. 1(a) for three different particle volume fractions: $\phi = 0.05$, $\phi = 0.30$, and $\phi = 0.40$. These curves are generated from calculations using the Percus-Yevick approximation, a standard analytic approach to calculations of $S(q)$ for monodisperse hard spheres [17]. The abscissa covers the range of dimensionless wave vectors $y = qa$ relevant to our systems. We use micron-sized charged polystyrene spheres in water with sufficient ionic content (0.01 molar) to screen the Coulomb interactions over roughly 4 nm. Thus, the interactions between the spheres in our samples are reasonably well approximated by a hard-core repulsive potential.

We will use DTS to extract information about $S(q)$ from wavelength dependence of l^*. Insight into how $l^*(\lambda)$ depends on $S(q)$ may be gained by considering the upper cutoff of the integral in Eq. (6). The upper cutoff, $2k_0 a$, is proportional to the ratio of the particle radius to the photon wavelength. Thus, for a *fixed* particle size, the value of l^* at photon wavelengths $\lambda_1 = 2\pi/k_1$ and $\lambda_2 = 2\pi/k_2$ depends on the behavior of $S(q)$ between the dimensionless wave vectors $2k_1 a$ and $2k_2 a$.

IV. EXPERIMENT

Our experimental goal is to determine l^* as a function of wavelength. There are a number of approaches to measuring l^* in a highly multiply scattering material. The simplest approach, discussed below, is to measure the transmission coefficient of a slab of colloid [1,8,9,12,18]. More complicated techniques to determine l^*, which may be more applicable to samples which absorb light, include the measurement of the angular width of the coherent backscattering cone [10,19–21] as well as measurements of the temporal broadening of a pulse of light during transmission through the colloid [22–24].

The transmission coefficient of a slab of colloid is the simplest quantity to measure since it requires neither pulsed lasers, nor collimated light sources, nor detectors with fine temporal or spatial resolution. The transmission coefficient is also fairly simple to interpret. For a slab of colloid with thickness L and transport mean free

path l^*, in the low absorption limit the diffuse light transmission coefficient is

$$T = \left(\frac{l^*}{L}\right) \frac{\frac{2}{3}\left(\frac{1+R}{1-R}\right) + \alpha}{1 + \frac{4}{3}\left(\frac{1+R}{1-R}\right)\frac{l^*}{L}}, \qquad (7)$$

where α is a parameter of the diffuse model of photon transport which is roughly unity [1,12,13,25] and R is the diffuse reflection coefficient from the colloid-glass-air boundary which contains the sample. This result is obtained by solving the one dimensional diffusion equation which describes photon transport through a slab of infinite transverse extent and comparing the transmitted to the reflected flux. The diffuse reflection coefficient is obtained from an angular average of the Fresnel reflection coefficient at the glass-colloid interface [26] and a sum over multiple reflections [12]. The approximately linear dependence of the diffuse-transmission coefficient on the photon transport mean free path (7) is experimentally ensured by keeping the ratio of L to l^* large and minimizing the reflection coefficient by submerging the sample cell in an index matching fluid (e.g., water).

Our apparatus for measuring the wavelength-dependent transmission coefficient (Fig. 2) uses a tungsten lamp, a monochrometer, an integrating sphere, and a silicon photodiode. This apparatus could probably be implemented simply by making small changes to a commercial spectrophotometer fitted with an integrating sphere. The integrating sphere allows us to collect light uniformly from many output angles. The light passing into the monochrometer is modulated using a chopper; a lock-in amplifier is used to measure the photocurrent
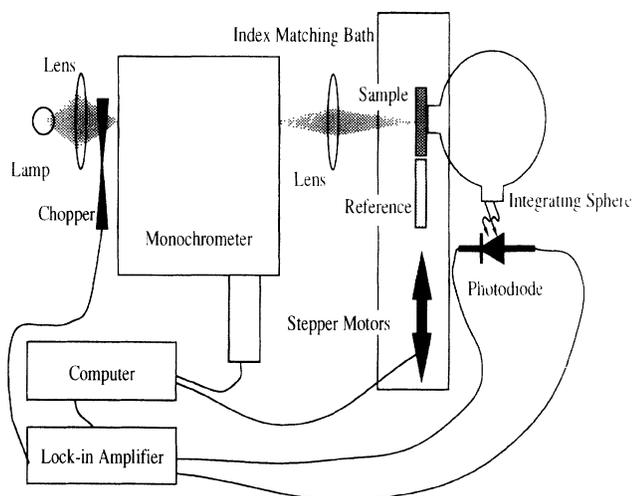
FIG. 2. Apparatus for diffuse-transmission spectroscopy. Computer controlled stepper motors switch between sample and reference cells and change the photon wavelength. Detection is accomplished using a lock-in amplifier and chopping the light entering the monochrometer. The sample is immersed in water to reduce the diffuse reflection coefficient. Note the similarity of this apparatus to commercially available spectrophotometers fitted with an integrating sphere.

at the chopper frequency from an unbiased photodiode. The system responds linearly over a range of transmission coefficients from 1 to at least 10^{-4}. The sample is immersed in water reducing the diffuse reflection coefficient from roughly 0.10 to 0.02 [12]. The integrating sphere is constructed of Spectralon reflectance material from Lab Sphere (North Sutton, New Hampshire). Spectralon is hydrophobic and can be immersed in water without changing its reflective properties; however, after submerging the entire sphere, we found that the photon path lengths in the sphere were so long that the weak photon absorption of *water in the integrating sphere* overwhelmed the signal from the colloid [27]. We, therefore, choose to hold the sample horizontally completely under water and we immerse only the input port of the *integrating sphere* in water, retaining the advantages of index matching. The cell thickness L was typically 1 or 2 mm so that the photon absorption was very small over the wavelength range probed.

Accurate absolute measurements of transmission require the measurement of a reference signal. In this experiment, normalization was accomplished by sequentially measuring the transmission through two samples, the one under study and another consisting of the same colloid at a significantly lower volume fraction where the structure factor is relatively less important and better understood [compare the solid and dashed lines in Fig. 1(a)]. The spectrum of the less dense colloid will have many of the same variations with wavelength as the sample, including variations of the form factor, the lamp intensity, and the detector efficiency. The reference cell will also have a similar angular output distribution of transmitted light as the sample under study. By using this normalization scheme, we produce a data set with *no adjustable experimental parameters*. If a nondiffuse sample is used for normalization, there will be an adjustable parameter, the angular collection efficiency. In this case, uncertainty in the collection efficiency will obscure the most sensitive feature of the data set, the absolute transmission. The final advantage of using a diffuse sample for normalization is that the uncertainty in the numerical values of R and α in the numerator of the relation between T and l^* (7) is normalized out of the data. In the data presented here, we ensure the applicability of the diffusion approximation by choosing reference samples such that L/l^* is always greater than 10 [12,24]. The data were obtained between 450 nm and 850 nm. The lower wavelength limit was set by the characteristic spectral response of our lamp, monochrometer, and photodiode; the upper wavelength limit was set by a weak photon absorption band in water.

We now discuss some of the experimental details of the DTS technique. While these details must be considered, they contribute very little to the final DTS spectrum and do not affect our interpretation of DTS data. A consideration of these issues, however, highlights the importance of the use of a suitable reference sample. Once a photon enters the integrating sphere, the probability that it will strike the detector is independent of the initial direction of the photon. Since the input and output ports on the integrating sphere are the same size, the photon is just as likely to return to the sample as it is to strike the pho-

todiode. The transmission coefficient is always much less than one, so most of the light returning to the sample will be reflected back into the integrating sphere. There is a finite probability, however, that a photon will escape after reentering the sample. By considering the possibility of a photon escaping after any number of reflections, we find that the measured transmission coefficient of the colloid in its cell T_m is related to the transmission coefficient of the colloid alone T by

$$T_m = \frac{cT/2}{1 - c(1-T)/2},$$ (8)

where c is the collection efficiency of the integrating sphere. The collection efficiency is essentially the solid angle subtended by the input aperture of the sphere divided by 2π. A conservative estimate of c in the present apparatus is between 0.75 and 0.80.

The quantity measured in DTS is the ratio of transmissions of two cells T_r/T_s, the reference and sample cells. Using the transmission calculated from the diffusion Eq. (7) and the correction due to multiple reflections from the integrating sphere off the sample cell (8), we arrive at the measured quantity

$$\frac{T_r}{T_s} = \frac{l_r^*}{l_s^*} \left(\frac{1 + \frac{4}{3}\frac{1+R}{1-R}\frac{l_s^*}{L}}{1 + \frac{4}{3}\frac{1+R}{1-R}\frac{l_r^*}{L}} \right) \frac{1 - c(1 - T_s)}{1 - c(1 - T_r)} .$$ (9)

To first order in l^*/L, this simplifies to

$$\frac{T_r}{T_s} = \frac{l_r^*}{l_s^*} \left(\frac{1 + Al_s^*/L}{1 + Al_r^*/L} \right) ,$$ (10)

where

$$A = (1 - c/2)\frac{4}{3}\left(\frac{1+R}{1-R}\right) + \left(\frac{2}{3}\frac{1+R}{1-R} + \alpha\right)c/2 .$$ (11)

The exact value of A is not known accurately, but is close to 1.5 (for $c = 0.8$, $R = 0.03$, and $\alpha = 1$). The normalized DTS spectrum will change by only a few percent

depending on the precise value of A. This uncertainty has little effect on our interpretation of the data. *Unnormalized* measurements, however, depend strongly on all three factors: the collection efficiency c, the diffuse reflection coefficient R, and the correct value of α, which in turn depends on the size of the scattering particles [10].

A final technical point is the calculation of the form factor $F(q, k_0 a)$ for which we use Mie theory [1]. The form factor depends strongly on the ratio of indices of refraction of the particle and of the continuous medium. For the index of refraction of water, we rely on the data from Ref. [27]. The refractive index of polystyrene is obtained from Refs. [28,29].

V. RESULTS

A. Influence of $S(q)$ on $l^*(\lambda)$

Using nearly hard-sphere polystyrene particles in water, we have tested the principles of DTS. Three systems with particle diameters between 205-nm and 460-nm and volume fractions of about 0.30 were studied (see Table I for details including absolute values of l^* at $\lambda = 500$ nm). Each particle size allows us to probe a different region of the hard-sphere structure factor because the value of the dimensionless wave vector $y = qa$ spanned for each particle size is different.

The sensitivity of DTS to interparticle structure is demonstrated in Fig. 3, where we plot $l_{sam}^*(y)/l_{ref}^*(y)$ measured for the three systems along with calculations based on Mie scattering theory and the Percus-Yevick approximation for $S(q)$. In these plots, $y = (4\pi a/\lambda)\, n(\lambda)$, where λ is the wavelength of light (in air) selected by the monochrometer, $n(\lambda)$ is the index of refraction of water at λ, and a is the particle radius. The experimental values of $l_{sam}^*(y)/l_{ref}^*(y)$ are obtained from measurements of the ratio between the transmission coefficient of the sample under investigation and that of a relatively dilute reference sample for which $S(q)$ is close to 1 (see Table I). The cal-
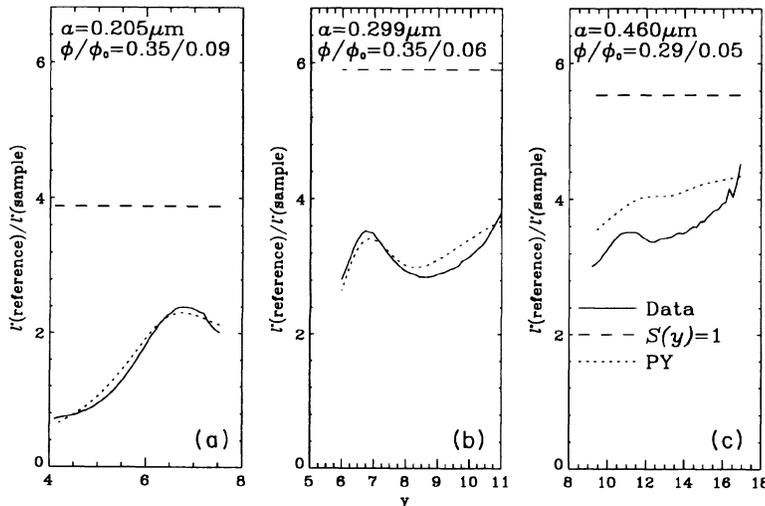
FIG. 3. Direct comparison of diffuse-transmission spectrum with Percus-Yevick calculation for three different samples. (a) $a = 205$ nm, $\phi_{sam} = 0.349$, $\phi_{ref} = 0.090$; (b) $a = 299$ nm, $\phi_{sam} = 0.354$, $\phi_{ref} = 0.060$; (c) $a = 460$ nm, $\phi_{sam} = 0.299$, $\phi_{ref} = 0.054$. A calculation ignoring structure is included in the dashed lines. The separation between the dashed and dotted lines indicates how strongly the diffuse-transmission spectrum depends on structure. There are no adjustable parameters in this graph; this is a comparison, not a fit.

TABLE I. To probe different length scales, we study three systems with different particle diameters. The calculated value of l^* at a wavelength of 500 nm is included.

Diameter (nm)	Sample ϕ	l^* (μm)	Reference ϕ	l^* (μm)
205	0.349	9.8	0.090	24.9
299	0.354	9.2	0.060	34.0
460	0.299	9.2	0.054	40.7

culations plotted in Fig. 3 are based on Eq. (6) using the parameters appropriate to each sample. We emphasize that there are no adjustable parameters in these plots; they directly compare measurements and theory. From these plots, we see that the Percus-Yevick structure factor does a remarkably good job of matching the relative value of l^* between different sample concentrations. Furthermore, we see that structure plays a significant role in the diffuse-transmission data set. In particular, if the structure factor were flat $[S(q) = 1]$, these curves would be horizontal lines (dashed in Fig. 3) with an ordinate equal to the ratio of the volume fractions of the sample and reference. In addition to the agreement in magnitude between the data and the calculations, there is good agreement in the location and direction of the bends and curves in the 205-nm and 299-nm systems. By contrast, the agreement between the data and the calculations for the largest (460-nm) system is much poorer. There are several plausible reasons for the good agreement in the case of two smaller spheres and the poor agreement in the case of the largest spheres. First, for our calculations of $l^*(y)$ we rely on our knowledge of the structure factors $S(y)$ for y values between zero and $2k_0a$. For the 205-nm and 300-nm systems, this means that $S(y)$ is probed only up to the first peak in the structure factor; for the larger 460-nm system, however, the second peak in $S(y)$ is also probed. Thus, more accurate knowledge of $S(y)$ over a larger range of y is required for the large spheres than is required for the small spheres in order to obtain a good description of the data. Second, the second peak in $S(y)$ corresponds to a much shorter length scale than does the first peak. At these shorter length scales, deviations from a strictly hard-sphere potential are expected. The small polydispersity which is found in latex colloids will also have a stronger effect on the second than on the first peak in $S(y)$. Thus, our results can be taken as an indication that the Percus-Yevick calculation of $S(y)$ for hard spheres is not an accurate model for the 460-nm system, that is, for values of qa greater than 10. Third, it is possible that l is too short in the 460-nm system, and that Eq. (6) is not valid for this system when the photon wavelength is less than 700 nm.

B. Particle sizing

The DTS spectrum can be a powerful tool for particle sizing. In Fig. 4, we plot the location of the peak in the DTS spectrum along with the calculated peak position (from the Percus-Yevick approximation) for different size particles. The peak positions are obtained by finding the
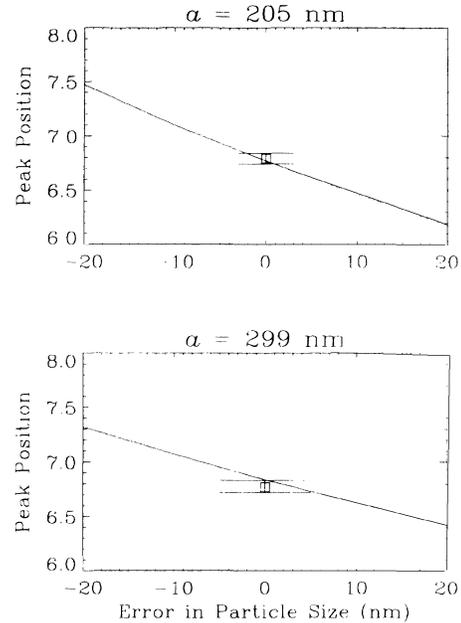
FIG. 4. Sensitivity of DTS to particle size. The most sensitive feature to match with these data sets is the first peak in the DTS spectrum where l^*_{ref}/l^*_{sam} has zero slope. The calculated peak (solid line) matches the measured peak position quite closely. By matching of this peak, particle size can be determined with 5% accuracy.

value of y at which the slope $[dl^*/d(k_0a)]$ of the transmission data from Fig. 3 is zero. The same examination of the position of zero slope of calculated data for different particle sizes is used to obtain the solid line in Fig. 4. The position of this peak is the most size-dependent feature of the spectrum. We see in this figure, that DTS can be used to estimate particle size to within 5%. This size resolution should be attainable for all samples in which the first peak in the structure factor is included in the scan range. In hard sphere systems, the peak in the structure factor scales with particle diameter. In contrast, in systems where the repulsion between particles is much larger than kT at a distance of the average interparticle spacing, the lattice constant will scale with $\phi^{-1/3}$ and we expect the first peak in the DTS spectrum to follow this scaling. Incidentally, in the course of this experiment, we used this technique to identify a 7% error in the particle size stated by the manufacturer of the 299-nm particles. This sizing error was verified by dynamic light scattering and electron microscopy.

C. Influence of different interparticle potentials

By comparing the diffuse-transmission spectra of samples that are identical except for their interparticle interaction potential, we highlight the dependence of the DTS spectrum on particle structure. A charged suspension of polystyrene spheres was prepared by rinsing 205-nm particles over ion-exchange resin. This effectively removes

TABLE II. Samples used in Fig. 5 with 205-nm particle diameter. All samples appeared white, not opalescent.

Sample ϕ	Ion concentration (mM)	Screening length (Å)
0.152	9.7	44
0.136	5.9	56
0.149	1.0	136
0.149	0.51	190

all excess counter ions from the suspension causing the formation of a colloidal crystal due to the electrostatic repulsion between the colloidal particles. After formation of the crystal, known concentrations of ions were obtained by diluting the crystal with a solution of NaCl. Four samples were prepared at the same volume fraction, but with different ionic content (Table II). The interparticle potential in this case is generally modeled as Debye-Hückel with a screening length l_{sc} that depends on the ionic strength of the solution ($l_{sc} \approx 3.0/\sqrt{[I]}$ Å [30]). The diffuse-transmission spectrum was measured using the most hard-sphere-like (smallest l_{sc}) sample as the reference. If the interparticle potential was not changed by changing the salt concentration, the measured DTS spectrum would be flat and equal to one. By contrast, we see in Fig. 5 that the interparticle potential dramatically and progressively changed as the ion content increased. Further, for stronger interactions (fewer ions) the structure is more pronounced as seen by the greater curvature in the spectrum taken at the lowest salt concentration. These were all noncrystalline samples which appeared white, not opalescent, to the eye. Their diffuse
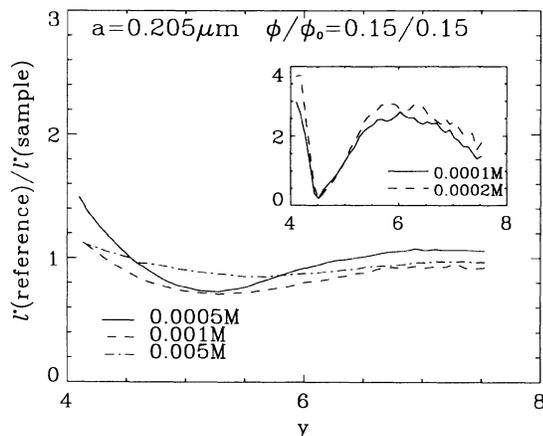
FIG. 5. The dependence of diffuse transmission on interaction potential is seen by comparing measurements made with samples with different screening lengths. The reference sample for these data sets had the same concentration of particles, but a shorter screening length. If there were no change in structure, or if DTS were not sensitive to such a change, the spectra would be flat lines. The progressive changes with increasing screening length demonstrate the sensitivity of DTS to interparticle potential. The screening length is approximately $3.0/\sqrt{[I]}$ Å, where the ion concentration $[I]$ is in units of moles per liter.

transmission spectra, however, highlight their structural differences. In the event of crystallization, it is known that there will be peaks in the DTS spectrum [31], which we have observed in our apparatus (see inset of Fig. 5). The diffusion approximation, however, does not always apply to colloidal crystals. Further work with different analytic tools is necessary for crystalline samples.

D. Effect of Volume Fraction

Diffuse transmission at a single wavelength has been used previously to determine l^* as a function of volume fraction [9,10]. At low volume fractions, l^* is proportional to ϕ and for large particles, where $k_0 a \gg 1$, l^* is proportional to ϕ even at fairly high volume fractions. Measurements of the dependence of diffuse transmission on volume fraction for a given system can easily be calibrated and then used for system characterization. When determining volume fraction by measuring transmission at a single wavelength, it is possible to be misled by changes in particle size or interparticle potential. By monitoring the diffuse-transmission spectrum, such changes can be ruled out. *Generally, horizontal shifts in the DTS spectrum indicate changes in particle size; vertical shifts indicate changing concentration. Changes in the shape of the spectrum indicate a change in the interparticle potential.*

E. Inverting $l^*(\lambda)$ to obtain $S(q)$

Ideally, the DTS data set could be inverted to provide not just comparisons with model calculations, but complete structure factors. We briefly present our attempts at inverting the DTS spectrum. A more complete discussion can be found in Ref. [32]. Inverting the equation for l^* as a function of dimensionless wave vector $k_0 a$ (6) is a difficult problem. The complexity of the Mie scattering expression for the form factor and its dependence on $k_0 a$ prevent any simple analytic inversion. Furthermore, attempts to obtain the structure factors from unconstrained inversion of the data give rapidly varying unphysical structure functions.

In order to restrict $S(y)$ to more physical values while performing a meaningful inversion, we have examined expansions of the structure factor of the form

$$S(y) = a_0 f_0(y) + a_1 f_1(y) + a_2 f_2(y) + \cdots , \qquad (12)$$

where the weights in the expansion $\{a_i\}$ determine $S(y)$, and the functions $f_i(y)$ are chosen based on our knowledge about the sample (e.g., particle size, interparticle potential). Our knowledge is imperfect, however, and our choices for the functions $f_i(y)$ are, in the end, somewhat arbitrary. We have focused on fits in which $f_0(y)$ is the Percus-Yevick structure factor that we compared directly to the data in Fig. 3. Further terms in the expansion were alternately chosen to be powers of y, spherical Bessel functions, and Percus-Yevick structure factor calculated for different particle sizes. All of these functions
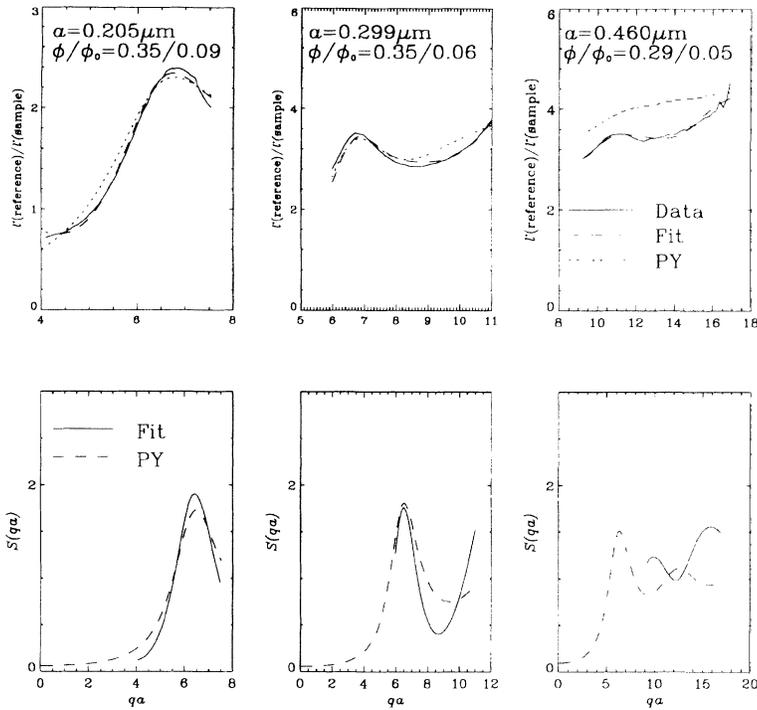
FIG. 6. The diffuse-transmission spectrum is fit with a structure function composed of the Percus-Yevick structure functions plus a polynomial. Over the range that we make measurements, the fits are reasonably good.

gave qualitatively similar results. In Fig. 6, we plot the fits and associated structure functions for $f_{i>1} = y^{i-1}$. We see good qualitative agreement with our data; the fits suggest that the first peak in $S(y)$ is somewhat sharper than the Percus-Yevick prediction. We also note a tendency of the fits to diverge for qa near zero. This can be easily understood to be a consequence of the y^3 weighting in Eq. (6), which makes the calculation of l^* very insensitive to the behavior of the structure factor at small y.

We estimate the sensitivity of this fitting procedure technique by applying it to calculated data for the Percus-Yevick structure function with added noise. Two types of noise are included: systematic noise is introduced through a several percent variation in the height of the curve, and point by point noise with a smaller amplitude is also added. By fitting them to many simulated noisy spectra, an estimate can be made of the sensitivity of DTS to noise and experimental errors. In Fig. 7, we plot the best polynomial fits to our data along with the one standard deviation limits on the Percus-Yevick structure function based on inversion of noisy calculated data sets. The measured structure function for the smaller systems (205 and 299 nm) falls just outside the expected range, indicating that the first peak in $S(y)$ is somewhat sharper than the Percus-Yevick $S(y)$. In the larger system, the disagreement cannot be attributed to the types
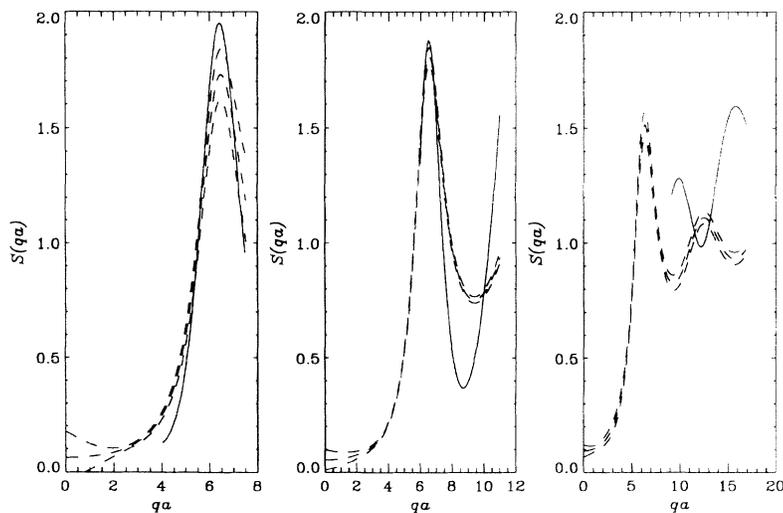
FIG. 7. The best fit $S(y)$ from a polynomial expansion of $S(y)$ (solid lines) is presented along with the one-standard deviation limits on the range of measured structures (dashed lines), assuming the Percus-Yevick structure was correct. From left to right, plots are for the 0.205-, 0.299-, and 0.460-μm systems.

of noise considered here.

We have also used this noise calculation to determine the number of parameters that can be usefully fit to the data. By repeating inversions of noisy calculated data and then fitting them to different numbers of parameters, we have found that the uncertainty in $S(y)$ increases dramatically when more than four parameters are used in the fit. That is, in fits to five or more parameters, the fits display greater sensitivity to the noise than to the underlying shape of the data set. This limit on the number of useful parameters matches our experience of fitting many sets of measured data.

VI. CONCLUSION

The diffuse-transmission spectrum is a sensitive indicator of structure in optically dense colloidal systems. Diffuse-transmission spectroscopy is especially useful near the first peak in $S(y)$. For higher order peaks, however, the averaging process of diffuse transmission obscures the shape of $S(y)$, making the structure function difficult to recover. It is also clear that DTS can be used in a variety of systems to monitor changes in composition, concentration, and interaction potential without dilution. Diffuse-transmission spectroscopy provides a less ambiguous signal of these changes than transmission measurements at a single wavelength, making it possible to distinguish between changes in interaction potential, particle size, and concentration. Further work is necessary on techniques for inverting diffuse-transmission data and the application of diffuse transmission to more systems.

[1] A. Ishimaru, in *Wave Propagation and Scattering in Random Media* (Academic Press, New York, 1978).

[2] C. F. Bohren, Am. J. Phys. **55**, 524 (1987).

[3] M. A. O'Leary, D. A. Boas, B. Chance, and A. G. Yodh, Phys. Rev. Lett. **69**, 2658 (1993).

[4] D. A. Boas, M. A. O'Leary, B. Chance, and A. G. Yodh, Phys. Rev. E **47**, R2999 (1993).

[5] D. J. Durian, D. A. Weitz, and D. J. Pine, Science **252**, 686 (1991).

[6] P. D. Kaplan, A. G. Yodh, and D. F. Townsend, J. Colloid Interf. Sci. **155**, 31 (1993).

[7] D. G. Dalgleish and D. S. Horne, Milchwissenschaft **46**, 417 (1991).

[8] A. Z. Genack, Phys. Rev. Lett. **58**, 2043 (1987).

[9] P. D. Kaplan, A. G. Yodh, and D. J. Pine, Phys. Rev. Lett. **68**, 393 (1992).

[10] S. Fraden and G. Maret, Phys. Rev. Lett. **65**, 512 (1990).

[11] X. Qiu et al., Phys. Rev. Lett. **65**, 516 (1990).

[12] P. D. Kaplan, M. H. Kao, A. G. Yodh, and D. J. Pine, Appl. Opt. **32**, 3828 (1993).

[13] D. J. Pine, D. A. Weitz, J. X. Zhu, and E. Herbolzheimer, J. Phys. I **51**, 2101 (1990).

[14] A. G. Yodh et al., Mol. Cryst. Liq. Cryst. Sci. Technol.— Sect. B **3**, 149 (1992).

[15] M. H. Kao, A. G. Yodh, and D. J. Pine, Phys. Rev. Lett. **70**, 242 (1992).

[16] J. X. Zhu et al., Phys. Rev. Lett. **68**, 2559 (1992).

[17] M. S. Wertheim, Phys. Rev. Lett. **10**, 321 (1963).

[18] P. W. Anderson, Philos. Mag. B **52**, 505 (1985).

[19] E. Akkermans, P. E. Wolf, R. Maynard, and G. Maret, J. Phys. **49**, 77 (1988).

[20] M. Kaveh, M. Rosenbluh, I. Edrei, and I. Freund, Phys. Rev. Lett. **57**, 2049 (1986).

[21] P. E. Wolf and G. Maret, Phys. Rev. Lett. **55**, 2696 (1985).

[22] J. M. Drake and A. Z. Genack, Phys. Rev. Lett. **63**, 259 (1989).

[23] A. G. Yodh, P. D. Kaplan, and D. J. Pine. Phys. Rev. B **42**, 4744 (1990).

[24] K. M. Yoo, F. Liu, and R. R. Alfano, Phys. Rev. Lett. **64**, 2647 (1990); **65**, 220(E) (1990).

[25] J. H. Li, A. A. Lisyansky, T. D. Cheung, D. Livdan, and A. Z. Genack, Europhys. Lett. **22**, 675 (1993).

[26] J. X. Zhu, D. J. Pine, and D. A. Weitz, Phys. Rev. A **44**, 3948 (1991).

[27] G. Hale and M. Querry, Appl. Opt. **12**, 555 (1973).

[28] L. H. Garcia-Rubio (private communication).

[29] T. Inagaki, E. T. Arakawa, R. N. Hamm, and M. W. Williams, Phys. Rev. B **15**, 3243 (1977).

[30] X. Qiu, Ph.D. thesis, University of Pennsylvania, 1990.

[31] Y. Monovoukas, G. G. Fuller, and A. P. Gast, J. Chem. Phys. **93**, 8294 (1990).

[32] P. D. Kaplan, Ph.D. thesis, University of Pennsylvania, 1993.

FIG. 2. Apparatus for diffuse-transmission spectroscopy. Computer controlled stepper motors switch between sample and reference cells and change the photon wavelength. Detection is accomplished using a lock-in amplifier and chopping the light entering the monochrometer. The sample is immersed in water to reduce the diffuse reflection coefficient. Note the similarity of this apparatus to commercially available spectrophotometers fitted with an integrating sphere.